

Electrically tunable spin injector free from the impedance mismatch problem

K. Ando*,¹ S. Takahashi,^{1,2} J. Ieda,^{2,3} H. Kurebayashi,⁴ T. Trypiniotis,⁴ C. H. W. Barnes,⁴ S. Maekawa,^{2,3} and E. Saitoh^{1,2,3}

¹*Institute for Materials Research, Tohoku University, Sendai 980-8577, Japan*

²*CREST, Japan Science and Technology Agency,
Sanbancho, Tokyo 102-0075, Japan*

³*The Advanced Science Research Center,
Japan Atomic Energy Agency, Tokai 319-1195, Japan*

⁴*Cavendish Laboratory, University of Cambridge,
J. J. Thomson Avenue, Cambridge CB3 0HE, United Kingdom*

* ando@imr.tohoku.ac.jp

Injection of spin currents into solids is crucial for exploring spin physics and spintronics^{1,2}. There has been significant progress in recent years in spin injection into high-resistivity materials, e.g., semiconductors and organic materials, which uses tunnel barriers to circumvent the impedance mismatch problem³⁻¹⁴; the impedance mismatch between ferromagnetic metals and high-resistivity materials drastically limits the spin-injection efficiency¹⁵. However, because of this problem, there is no route for spin injection into these materials through low resistivity interfaces, i.e., ohmic contacts, even though it promises easy and versatile pathway for spin injection without the need for growing high-quality tunnel barriers. Here we show experimental evidence that spin pumping enables spin injection free from this condition; room-temperature spin injection into GaAs from Ni₈₁Fe₁₉ through an ohmic contact is demonstrated via dynamical spin exchange. Furthermore, we demonstrate that this exchange can be controlled electrically by applying a bias voltage across a Ni₈₁Fe₁₉/GaAs interface, enabling electric tuning of the spin-pumping efficiency.

Electron transport across a ferromagnetic metal/nonmagnetic material gives rise to nonequilibrium spin currents in the nonmagnetic layer. However, the spin polarization of the current across the interface is strongly reduced especially when the electrical resistance of these two layers is considerably different, e.g., a ferromagnetic metal/semiconductor (FM/SC) contact. This is known as the impedance mismatch problem^{3,15}.

The above problem arises from the fact that spins are injected by carrier transport across a FM/SC interface (see Fig. 1a). It seems natural to consider that this problem disappears when spins are injected directly into the SC layer without using charge transport across the interface (see Fig. 1b); the driving force for the spin flow (not the charge carrier flow) is expected to offer a way for versatile spin injection free from the impedance mismatch problem. In this work, we experimentally demonstrate that the spin pumping, generation of pure spin currents from magnetization precession¹⁶⁻¹⁸, provides a powerful way for direct spin injection. The spin-angular momentum of the precessing magnetization in the FM layer is transferred to the carriers in the SC layer via dynamical exchange interaction at the FM/SC interface, inducing a pure spin voltage, the potential acting on *spins* not on *carriers*, in the SC layer. This enables spin injection into both *p*- and *n*-doped GaAs from Ni₈₁Fe₁₉ through both ohmic and Schottky contacts in a Ni₈₁Fe₁₉/GaAs interface even at

room temperature. The ohmic contact case is the one showing the higher spin current injection in our experiments in contrast to the expectation in the case of spin injection by charge transport where the conductivity mismatch problem is present. Furthermore, the spin-pumping efficiency is demonstrated to be controlled electrically via electric modulation of the dynamical exchange interaction at the $\text{Ni}_{81}\text{Fe}_{19}/\text{GaAs}$ interface, providing a clear picture of the dynamical spin injection.

The room-temperature spin injection through ohmic and Schottky contacts is observed using the inverse spin-Hall effect (ISHE)¹⁹⁻²³. The ISHE converts a spin current into an electric voltage, enabling electric detection of the spin current. Figure 2a shows a schematic illustration of the samples used in this study. The samples are a $\text{Ni}_{81}\text{Fe}_{19}/\text{Zn-doped GaAs}$ (a $\text{Ni}_{81}\text{Fe}_{19}/p\text{-GaAs}$ film) with a doping concentration of $N_{\text{D}} = 1.4 \times 10^{19} \text{ cm}^{-3}$ and a $\text{Ni}_{81}\text{Fe}_{19}/\text{Si-doped GaAs}$ (a $\text{Ni}_{81}\text{Fe}_{19}/n\text{-GaAs}$ film) with $N_{\text{D}} = 1.2 \times 10^{18} \text{ cm}^{-3}$ (for details, see Methods). Here, note that the current-voltage characteristics shown in Figs. 2b and 2c indicate the formation of ohmic and Schottky contacts in the $\text{Ni}_{81}\text{Fe}_{19}/p\text{-GaAs}$ and $\text{Ni}_{81}\text{Fe}_{19}/n\text{-GaAs}$ interfaces, respectively.

We measured the ferromagnetic resonance (FMR) signal and the electric-potential difference V between the electrodes attached to the GaAs layer to detect spin injection; as shown in Fig. 2a, in the FMR condition, the dynamical exchange interaction drives the spin pumping, injecting pure spin currents into the GaAs layer through the ohmic and Schottky contacts. This spin current flows in the GaAs layer, giving rise to an electromotive force \mathbf{E}_{ISHE} in the GaAs layer via the ISHE. In the ISHE process, when the spin current carries the spin polarization $\boldsymbol{\sigma}$ along the spatial direction \mathbf{j}_s , \mathbf{E}_{ISHE} is given by²⁰

$$\mathbf{E}_{\text{ISHE}} \propto \mathbf{j}_s \times \boldsymbol{\sigma}. \quad (1)$$

Here, the dc component of $\boldsymbol{\sigma}$ is parallel to the magnetization-precession axis in the $\text{Ni}_{81}\text{Fe}_{19}$ layer and \mathbf{j}_s is along the normal direction to the film plane as shown in Fig. 2a²³. During the measurements, the $\text{Ni}_{81}\text{Fe}_{19}/\text{GaAs}$ sample was placed at the center of a TE_{011} microwave cavity with the frequency of $f = 9.46 \text{ GHz}$. An external static magnetic field \mathbf{H} was applied along the film plane (see Fig. 2a). All of the measurements were performed at room temperature.

Figures 3a and 3b show the FMR spectrum $dI(H)/dH$ and the dc electromotive force signals $V(\theta = 0)$ measured for the $\text{Ni}_{81}\text{Fe}_{19}/p\text{-GaAs}$ (black) and $\text{Ni}_{81}\text{Fe}_{19}/n\text{-GaAs}$ (red)

films under the 200 mW microwave excitation. Here, we define $V(\theta) \equiv (\tilde{V}^\theta - \tilde{V}^{\theta+180^\circ})/2$, the asymmetric component of V with respect to \mathbf{H} , which allows us to eliminate heating effects arising from the microwave absorption from the V spectra (see Methods). \tilde{V}^θ and $\tilde{V}^{\theta+180^\circ}$ are the electromotive force V measured when the external magnetic field is applied at an out-of-plane angle of θ and $\theta + 180^\circ$ to the film plane (see Fig. 3c), respectively. In the $V(\theta = 0)$ spectra, clear electromotive force signals are observed around the resonance field $H = H_{\text{FMR}}$ for both the $\text{Ni}_{81}\text{Fe}_{19}/p\text{-GaAs}$ and $\text{Ni}_{81}\text{Fe}_{19}/n\text{-GaAs}$ films.

The observed electromotive force signals are direct evidence for room-temperature spin injection into the GaAs layer through the ohmic and Schottky contacts; the electromotive force is attributed to the ISHE in the GaAs layer induced by the spin pumping. Notable is that the spectral shape of the electromotive force is well reproduced using a Lorentz function (see Fig. 3b), as expected for the ISHE induced by the spin pumping²⁰. This is confirmed also from the microwave power P_{MW} and out-of-plane magnetic field angle θ dependence of the electromotive force shown in Figs. 3f and 3k (see Supplementary Information sections A and B for details), providing further evidence for room-temperature spin injection into the GaAs layer through the ohmic and Schottky contacts.

The dynamical spin injection using spin pumping from the $\text{Ni}_{81}\text{Fe}_{19}$ layer into the GaAs layer is driven by the dynamical exchange interaction between a localized spin \mathbf{S} in the $\text{Ni}_{81}\text{Fe}_{19}$ layer and a spin \mathbf{s} of carriers in the GaAs layer at the $\text{Ni}_{81}\text{Fe}_{19}/\text{GaAs}$ interface: $H_{\text{ex}} = -J_{\text{ex}}\mathbf{S} \cdot \mathbf{s}$, where J_{ex} is the exchange interaction constant. By solving coupled equations for the magnetizations of the $\text{Ni}_{81}\text{Fe}_{19}$ and GaAs layers (the Landau-Lifshitz-Gilbert equation and the Bloch equation with spin diffusion)²⁴, in which the exchange torque arising from the exchange interaction is taken into account (see Supplementary Information section C for details), we obtain the pumped spin current at the interface: $j_s^{\text{sp}} = g_r^{\uparrow\downarrow}(e/2\pi\hbar)(\hbar/M_s^2) [\mathbf{M} \times d\mathbf{M}/dt]_z$, where $g_r^{\uparrow\downarrow} = (\pi\hbar/2e^2)(\sigma_N/\lambda_N)(a_c/\lambda_N)^2(SJ_{\text{ex}}\tau_N^{\text{sf}}/\hbar)^2$ is the spin-mixing conductance, which determines the spin-injection efficiency. Here, M_s is the saturation value of the magnetization \mathbf{M} . σ_N and λ_N are the electrical conductivity and the spin diffusion length of the GaAs layer, respectively. a_c and τ_N^{sf} are the average distance between carriers and the spin relaxation time of carriers in the GaAs layer, respectively. The z axis is defined in Fig. 2a. Using the measured values of the magnitude of the electromotive force $V_{\text{ISHE}}(\theta = 0)$ (see Fig. 3d), we find the spin-mixing conductance $g_r^{\uparrow\downarrow} = 3.7 \times 10^{18} \text{ m}^{-2}$ for the $\text{Ni}_{81}\text{Fe}_{19}/p\text{-GaAs}$ film and $g_r^{\uparrow\downarrow} = 1.5 \times 10^{17} \text{ m}^{-2}$ for the $\text{Ni}_{81}\text{Fe}_{19}/n\text{-GaAs}$ film (see

Supplementary Information section C for details). The corresponding spin current density for the Ni₈₁Fe₁₉/*p*-GaAs film is $j_s^{\text{sp}} = 3.3 \times 10^6$ A/m², which is comparable to the value $j_s^{\text{sp}} = 5.8 \times 10^6$ A/m² obtained in a Ni₈₁Fe₁₉/Pt film²³. This large amplitude of spin currents is several orders of magnitude larger than that obtained by the electrical spin injection through a tunnel barrier^{7,9} $\sim 10^3 - 10^4$ A/m², where a high resistivity interface limits the current density; the dynamical spin injection using the spin pumping enables high density spin injection with low energy carriers free from the impedance mismatch condition. The small spin-mixing conductance in the Ni₈₁Fe₁₉/*n*-GaAs system is mainly due to the existence of the Schottky barrier at the interface. In fact, $g_r^{\uparrow\downarrow}$ measured for a Schottky Ni₈₁Fe₁₉/*p*-GaAs ($N_D = 4.1 \times 10^{17}$ cm⁻³) interface $g_r^{\uparrow\downarrow} = 2.2 \times 10^{17}$ m⁻² (see Figs. 4b, 4c, and Supplementary Information section C) is smaller than that for the ohmic Ni₈₁Fe₁₉/*p*-GaAs interface.

The above experimental results suggest the possibility of electric control of the dynamical spin injection; the dynamical exchange interaction can be controlled by applying a bias voltage V_{in} across the interface (see Fig. 4a). In Fig. 4g, we show the band structure of the Schottky Ni₈₁Fe₁₉/*p*-GaAs interface with the bias voltage V_{in} . When $V_{\text{in}} < 0$, the depletion region and potential barrier increase, reducing spin exchange at the interface. In contrast, when $V_{\text{in}} > 0$, the depletion region and potential barrier decrease as shown in Fig. 4g, giving rise to strong exchange interaction. We measured the ISHE induced by the spin pumping in the Schottky Ni₈₁Fe₁₉/*p*-GaAs system with applying V_{in} across the interface.

Figure 4h shows the V_{in} dependence of the spin-mixing conductance $g_r^{\uparrow\downarrow}$ estimated from the magnitude of the measured voltage $V_{\text{ISHE}}(\theta = 0)$ with the assumption that electric field effects on spin diffusion are negligibly small, since the applied field is sufficiently small in this system²⁵. The spin-mixing conductance $g_r^{\uparrow\downarrow}$ decreases with decreasing V_{in} when $V_{\text{in}} < 0$. When $V_{\text{in}} > 0$, in contrast, $g_r^{\uparrow\downarrow}$ increases with the bias voltage V_{in} . These results are consistent with the above prediction; the dynamical exchange interaction is enhanced by reducing the barrier width and height. We confirmed that the saturation magnetization $4\pi M_s$ is independent of V_{in} as shown in Fig. 4e. This shows that heating effects are negligibly small in this measurement because heating decreases $4\pi M_s$ ²⁶. Current-induced effects, such as the ordinary Hall effect, are also irrelevant; the electric voltage is independent of V_{in} when $P_{\text{MW}} = 0$ (see Fig. 4d) and the observed change of $V_{\text{ISHE}}(\theta = 0)$ when $P_{\text{MW}} = 200$ mW is not linear to the bias current J (see Fig. 4f), confirming that the spin-pumping efficiency is controlled electrically by applying a bias voltage.

We demonstrated the versatility of the dynamical spin injection method by showing successful spin injection at room temperature with various cases, p - and n -type semiconductors through ohmic and Schottky interfaces using the same structure as in metallic systems; this method can be used as a versatile and powerful method for spin injection into a wide range of materials free from the impedance mismatch problem. We further provide a clear demonstration that dynamical spin injection can be controlled by applying a bias voltage, opening a route for a spin-current switch. Here, note that it is nontrivial that pure-spin-current injection is free from the impedance mismatch problem; e.g., the efficiency of spin injection using the spin-Hall effect in bilayer systems is limited by the impedance mismatch²⁶. Furthermore, even in a magnetic p - n junction where the impedance mismatch plays a minor role, a space-charge region prevents spin injection at low bias²⁷. Since the spin pumping method requires only magnetization precession in a FM/SC junction, this method can be combined with a wide range of FMR excitation elements, e.g., spin torque oscillators, enabling integration of this method into spintronics devices, such as semiconductor spin lasers¹. Thus, this new spin-injection approach will pave the way toward the creation of room-temperature spintronic devices in a large selection of materials, promising dramatic advances in the field of spintronics.

Methods

Measurements technique. The samples used in this study are $\text{Ni}_{81}\text{Fe}_{19}/p\text{-GaAs}$ and $\text{Ni}_{81}\text{Fe}_{19}/n\text{-GaAs}$ films comprising a 10-nm-thick ferromagnetic $\text{Ni}_{81}\text{Fe}_{19}$ layer and a 400- μm -thick GaAs layer, as illustrated in Fig. 2a. The $\text{Ni}_{81}\text{Fe}_{19}$ layer was evaporated in a high vacuum on a Zn-doped GaAs substrate (the $\text{Ni}_{81}\text{Fe}_{19}/p\text{-GaAs}$ film) with a doping concentration of $N_{\text{D}} = 1.4 \times 10^{19} \text{ cm}^{-3}$ and a Si-doped GaAs substrate (the $\text{Ni}_{81}\text{Fe}_{19}/n\text{-GaAs}$ film) with $N_{\text{D}} = 1.2 \times 10^{18} \text{ cm}^{-3}$. The surface of the $\text{Ni}_{81}\text{Fe}_{19}$ layer is of a $1.0 \times 2.5 \text{ mm}^2$ rectangular shape for the $\text{Ni}_{81}\text{Fe}_{19}/p\text{-GaAs}$ film and a $1.0 \times 2.0 \text{ mm}^2$ rectangular shape for the $\text{Ni}_{81}\text{Fe}_{19}/n\text{-GaAs}$ film, respectively. The surface of the GaAs layer was cleaned by chemical etching immediately before the evaporation²⁸. Two In-based ohmic contacts are attached to the ends of the GaAs layer as shown in Fig. 2a. The ratios of the electrical conductivity for the GaAs layer σ_{N} to that for the $\text{Ni}_{81}\text{Fe}_{19}$ layer σ_{F} , $\sigma_{\text{N}}/\sigma_{\text{F}} = 9.7 \times 10^{-3}$ (the $\text{Ni}_{81}\text{Fe}_{19}/p\text{-GaAs}$ film) and $\sigma_{\text{N}}/\sigma_{\text{F}} = 2.6 \times 10^{-2}$ (the $\text{Ni}_{81}\text{Fe}_{19}/n\text{-GaAs}$ film), show that the impedance mismatch problem is critical in these systems. The mismatch of the spin-diffusion length of the $\text{Ni}_{81}\text{Fe}_{19}$ layer and the GaAs layer also reduces the spin injection efficiency^{3,15}. The thick GaAs substrates ensure that the backflow spin currents are negligibly small in these systems¹⁷. The magnitude of the electromotive force due to the ISHE can be increased by reducing the thickness of the GaAs layer, since it reduces a short circuit current in the GaAs layer. The sample used for the electric control of the spin pumping is a $\text{Ni}_{81}\text{Fe}_{19}/p\text{-GaAs}$ system. The strong ISHE in p -doped GaAs allows sensitive detection of the spin pumping. The $\text{Ni}_{81}\text{Fe}_{19}/p\text{-GaAs}$ sample comprises a 10-nm-thick ferromagnetic $\text{Ni}_{81}\text{Fe}_{19}$ layer and a 400 μm -thick GaAs layer with the doping concentration of $N_{\text{D}} = 4.1 \times 10^{17} \text{ cm}^{-3}$. The Schottky barrier at the interface enables the electric tuning of the dynamical exchange interaction. The surface of the $\text{Ni}_{81}\text{Fe}_{19}$ layer is of a $1.0 \times 2.5 \text{ mm}^2$ rectangular shape. In the voltage measurements, we define the asymmetric component of the electromotive force $V(\theta)$ with respect to \mathbf{H} to eliminate thermoelectric effects due to small but finite asymmetry of the position of the electrodes attached to the GaAs layer with respect to the $\text{Ni}_{81}\text{Fe}_{19}$ layer.

-
- ¹ Žutić, I., Fabian, J. & Das Sarma, S. Spintronics: Fundamentals and applications. *Rev. Mod. Phys.* **76**, 323–410 (2004).
- ² Awschalom, D. D. & Flatté, M. E. Challenges for semiconductor spintronics. *Nat. Phys.* **3**, 153–159 (2007).
- ³ Rashba, E. I. Theory of electrical spin injection: Tunnel contacts as a solution of the conductivity mismatch problem. *Phys. Rev. B* **62**, R16267–R16270 (2000).
- ⁴ Zhu, H. J. *et al.* Room-temperature spin injection from Fe into GaAs. *Phys. Rev. Lett.* **87**, 016601 (2001).
- ⁵ Crooker, S. A. *et al.* Imaging spin transport in lateral ferromagnet/semiconductor structures. *Science* **309**, 2191–2195 (2005).
- ⁶ Appelbaum, I., Huang, B. & Monsma, D. J. Electronic measurement and control of spin transport in silicon. *Nature* **447**, 295–298 (2007).
- ⁷ Jonker, B. T., Kioseoglou, G., Hanbicki, A. T., Li, C. H. & Thompson, P. E. Electrical spin-injection into silicon from a ferromagnetic metal/tunnel barrier contact. *Nat. Phys.* **3**, 542–546 (2007).
- ⁸ Lou, X. *et al.* Electrical detection of spin transport in lateral ferromagnet-semiconductor devices. *Nat. Phys.* **3**, 197–202 (2007).
- ⁹ Dash, S. P., Sharma, S., Patel, R. S., de Jong, M. P. & Jansen, R. Electrical creation of spin polarization in silicon at room temperature. *Nature* **462**, 491–494 (2009).
- ¹⁰ Jiang, X. *et al.* Highly spin-polarized room-temperature tunnel injector for semiconductor spintronics using MgO(100). *Phys. Rev. Lett.* **94**, 056601 (2005).
- ¹¹ Xiong, Z. H., Wu, D., Vardeny, Z. V. & Shi, J. Giant magnetoresistance in organic spin-valves. *Nature* **427**, 821–824 (2004).
- ¹² Tombros, N., Jozsa, C., Popinciuc, M., Jonkman, H. T. & van Wees, B. J. Electronic spin transport and spin precession in single graphene layers at room temperature. *Nature* **448**, 571–574 (2007).
- ¹³ Lou, X. *et al.* Electrical detection of spin accumulation at a ferromagnet-semiconductor interface. *Phys. Rev. Lett.* **96**, 176603 (2006).
- ¹⁴ Tran, M. *et al.* Enhancement of the spin accumulation at the interface between a spin-polarized

- tunnel junction and a semiconductor. *Phys. Rev. Lett.* **102**, 036601 (2009).
- ¹⁵ Schmidt, G., Ferrand, D., Molenkamp, L. W., Filip, A. T. & van Wees, B. J. Fundamental obstacle for electrical spin injection from a ferromagnetic metal into a diffusive semiconductor. *Phys. Rev. B* **62**, R4790–R4793 (2000).
- ¹⁶ Tserkovnyak, Y., Brataas, A. & Bauer, G. E. W. Enhanced Gilbert damping in thin ferromagnetic films. *Phys. Rev. Lett.* **88**, 117601 (2002).
- ¹⁷ Brataas, A., Tserkovnyak, Y., Bauer, G. E. W. & Halperin, B. I. Spin battery operated by ferromagnetic resonance. *Phys. Rev. B* **66**, 060404(R) (2002).
- ¹⁸ Mizukami, S., Ando, Y. & Miyazaki, T. Effect of spin diffusion on Gilbert damping for a very thin permalloy layer in Cu/permalloy/Cu/Pt films. *Phys. Rev. B* **66**, 104413 (2002).
- ¹⁹ Bakun, A. A., Zakharchenya, B. P., Rogachev, A. A., Tkachuk, M. N. & Fleisher, V. G. Observation of a surface photocurrent caused by optical orientation of electrons in a semiconductor. *JETP Lett.* **40**, 1293–1295 (1984).
- ²⁰ Saitoh, E., Ueda, M., Miyajima, H. & Tatara, G. Conversion of spin current into charge current at room temperature: Inverse spin-Hall effect. *Appl. Phys. Lett.* **88**, 182509 (2006).
- ²¹ Kimura, T., Otani, Y., Sato, T., Takahashi, S. & Maekawa, S. Room-temperature reversible spin Hall effect. *Phys. Rev. Lett.* **98**, 156601 (2007).
- ²² Valenzuela, S. O. & Tinkham, M. Direct electronic measurement of the spin Hall effect. *Nature* **442**, 176–179 (2006).
- ²³ Ando, K. *et al.* Angular dependence of inverse spin–Hall effect induced by spin pumping investigated in a Ni₈₁Fe₁₉/Pt thin film. *Phys. Rev. B* **78**, 014413 (2008).
- ²⁴ Kajiwara, Y. *et al.* Transmission of electrical signals by spin-wave interconversion in a magnetic insulator. *Nature* **464**, 262–266 (2010).
- ²⁵ Yu, Z. G. & Flatté, M. E. Electric-field dependent spin diffusion and spin injection into semiconductors. *Phys. Rev. B* **66**, 201202(R) (2002).
- ²⁶ Ando, K. *et al.* Electric manipulation of spin relaxation using the spin Hall effect. *Phys. Rev. Lett.* **101**, 036601 (2008).
- ²⁷ Žutić, I., Fabian, J. & Das Sarma, S. Spin-polarized transport in inhomogeneous magnetic semiconductors: Theory of magnetic/nonmagnetic *p-n* junctions. *Phys. Rev. Lett.* **88**, 066603 (2002).
- ²⁸ Trypiniotis, T., Tse, D., Steinmuller, S., Cho, W. & Bland, J. Efficient spin detection across

the hybrid Co/GaAs Schottky interface. *IEEE Trans. Magn.* **43**, 2872–2874 (2007).

- ²⁹ Sze, S. M. & Ng, K. K. *Physics of Semiconductor Devices* (Wiley-Interscience, New York, 2006), 3rd edn.

Acknowledgements

This work was supported by the Cabinet Office, Government of Japan through its “Funding Program for Next Generation World-Leading Researchers,” a Grant-in-Aid for Research Activity Start-up (2284005) from MEXT, Japan, a Strategic Information and Communications R&D Promotion Program from MIC (102102001), Japan, a Grant-in-Aid for Scientific Research in Priority Area “Creation and control of spin current” (19048028, 19048009) from MEXT, Japan, a Grant-in-Aid for Scientific Research (A) (21244058) from MEXT, Japan, a Grant for Industrial Technology Research from NEDO, Japan, and the Next Generation Supercomputing Project of Nanoscience Program from IMS, Japan.

Author contributions

K.A. designed the experiment, collected all of the data, and performed analysis of the data. E.S. supervised the study. K.A., H.K. and T.T. fabricated the samples. K.A., S.T., J.I., H.K., C.H.W.B. and S.M. developed the explanation of the experiment. K.A. and S.T. wrote the manuscript. All authors discussed the results and commented on the manuscript.

Additional information

The authors declare no competing financial interests.

Figure 1: Spin injection via carrier transport and dynamical exchange interaction.

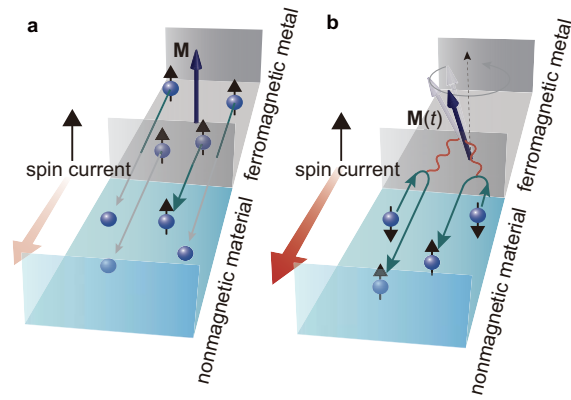
a, A schematic illustration of the conventional electrical spin injection in a nonmagnetic material/ferromagnetic metal junction. \mathbf{M} denotes the static magnetization. The spin current is driven by electron transport across the interface, which is drastically limited by the impedance mismatch. **b**, A schematic illustration of spin injection via dynamical exchange interaction in a nonmagnetic material/ferromagnetic metal junction. $\mathbf{M}(t)$ shows the precessing magnetization. The dynamical exchange interaction at the interface transfers the spin-angular momentum from the magnetization in the ferromagnetic layer to the electrons in the nonmagnetic layer, inducing a pure spin voltage in the nonmagnetic layer.

Figure 2: Dynamical spin injection and inverse spin-Hall effect.

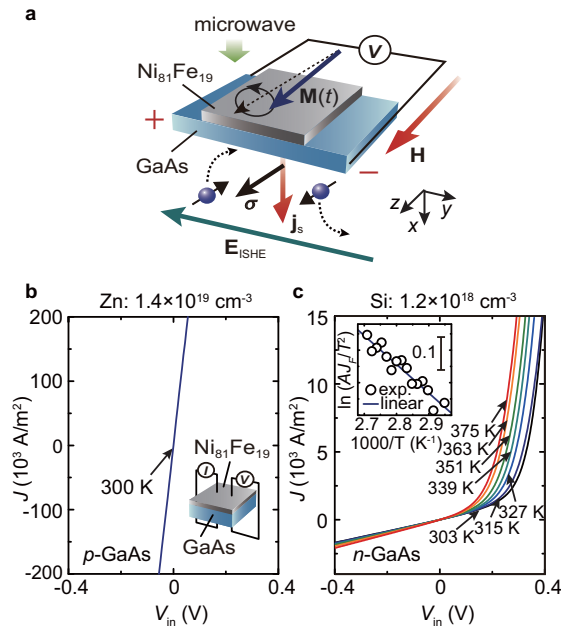
a, A schematic illustration of the inverse spin-Hall effect induced by the spin pumping in the $\text{Ni}_{81}\text{Fe}_{19}/\text{GaAs}$ system. \mathbf{H} and $\mathbf{M}(t)$ represent the external magnetic field and the magnetization in the $\text{Ni}_{81}\text{Fe}_{19}$ layer, respectively. \mathbf{E}_{ISHE} , \mathbf{j}_s , and $\boldsymbol{\sigma}$ denote the electromotive force due to the inverse spin-Hall effect, the spatial direction of the spin current, and the spin-polarization vector of the spin current, respectively. **b**, Bias voltage V_{in} dependence of current density J through the $\text{Ni}_{81}\text{Fe}_{19}/p\text{-GaAs}$ junction. **c**, Bias voltage V_{in} dependence of current density J through the $\text{Ni}_{81}\text{Fe}_{19}/n\text{-GaAs}$ junction for various temperatures T . J_{F} is the current density for the fixed bias $V_{\text{F}} = 0.13$ V. A is the electrically active area. The Schottky barrier height is found to be $\phi_{\text{S}} = 0.20$ eV from the temperature dependence of the forward bias current²⁹.

Figure 3: Measurements of spin injection. **a**, Field (H) dependence of the FMR signal $dI(H)/dH$ measured for the $\text{Ni}_{81}\text{Fe}_{19}/p\text{-GaAs}$ film when the external magnetic field \mathbf{H} is applied along the film plane ($\theta = 0$). Here, I denotes the microwave absorption intensity. H_{FMR} is the resonance field. $H_{\text{FMR}} = 111$ mT for the $\text{Ni}_{81}\text{Fe}_{19}/p\text{-GaAs}$ film and $H_{\text{FMR}} = 121$ mT for the $\text{Ni}_{81}\text{Fe}_{19}/n\text{-GaAs}$ film, respectively. **b**, Field dependence of the electromotive force $V(\theta = 0)$ measured for the $\text{Ni}_{81}\text{Fe}_{19}/p\text{-GaAs}$ (black) and $\text{Ni}_{81}\text{Fe}_{19}/n\text{-GaAs}$ (red) films under the 200 mW microwave excitation. Here, $V(\theta) \equiv (\tilde{V}^\theta - \tilde{V}^{\theta+180^\circ})/2$, where \tilde{V}^θ and $\tilde{V}^{\theta+180^\circ}$ are the electromotive force V measured when \mathbf{H} is applied at an angle of θ and $\theta + 180^\circ$ to the film plane (see **c**), respectively. The open circles are the experimental data. The solid curve shows the fitting result using a Lorentz function. **c**, The definition of the out-of-plane-magnetic field angle θ and magnetization angle ϕ . **d**, The definition of the magnitude of the electromotive force V_{ISHE} . **e**, Field dependence of $V(\theta = 0)$ measured for the $\text{Ni}_{81}\text{Fe}_{19}/p\text{-GaAs}$ at different microwave excitation power. **f**, Microwave power P_{MW} dependence of $V_{\text{ISHE}}(\theta = 0)$. The solid circles are the experimental data. The solid lines show the linear fit to the data. **g**, Magnetic field angle θ dependence of the FMR signal $dI(H)/dH$ for the $\text{Ni}_{81}\text{Fe}_{19}/p\text{-GaAs}$ film. **h**, Magnetic field angle θ dependence of $V(\theta)$ for the $\text{Ni}_{81}\text{Fe}_{19}/p\text{-GaAs}$ film. **i**, Magnetic field angle θ dependence of H_{FMR} measured for the $\text{Ni}_{81}\text{Fe}_{19}/p\text{-GaAs}$ film. The filled circles represent the experimental data. The solid curve is the numerical solution of the equilibrium and resonance conditions (see Supplementary Information section B for details). **j**, Magnetic field angle θ dependence of ϕ for the $\text{Ni}_{81}\text{Fe}_{19}/p\text{-GaAs}$ film estimated from the equilibrium condition. **k**, Magnetic field angle θ dependence of $V_{\text{ISHE}}(\theta)/V_{\text{ISHE}}(\theta = 0)$. The solid circles are the experimental data. The solid curve is the theoretical curve (see Supplementary Information section B).

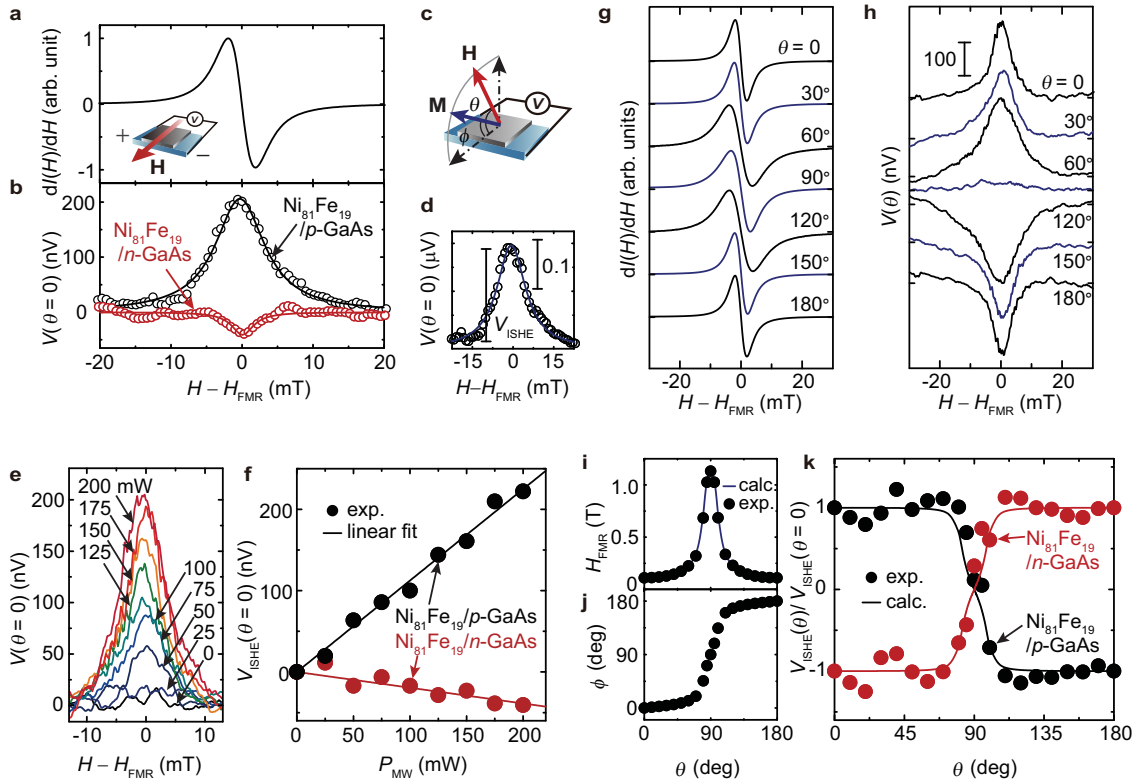
Figure 4: Electric control of dynamical spin injection. **a**, A schematic illustration of the $\text{Ni}_{81}\text{Fe}_{19}/p\text{-GaAs}$ system. V_{in} represents the bias voltage applied to the system. **b**, Field (H) dependence of the electromotive force $V(\theta = 0)$ measured for the $\text{Ni}_{81}\text{Fe}_{19}/p\text{-GaAs}$ ($N_{\text{D}} = 4.1 \times 10^{17} \text{ cm}^{-3}$) system under the 200 mW microwave excitation. The open circles are the experimental data. The solid curve shows the fitting result using a Lorentz function. $H_{\text{FMR}} = 106 \text{ mT}$ is the resonance field. **c**, Bias voltage V_{in} dependence of current density J through the $\text{Ni}_{81}\text{Fe}_{19}/p\text{-GaAs}$ junction at $P_{\text{MW}} = 0$. The Schottky barrier height is estimated to be $\phi_{\text{S}} = 0.43 \text{ eV}$. **d**, Bias voltage V_{in} dependence of the magnitude of the electromotive force $V_{\text{ISHE}}(\theta = 0)$ at $P_{\text{MW}} = 0$: $V_{\text{ISHE}}^{P_{\text{MW}}=0}$. The solid line shows $V_{\text{ISHE}}^{P_{\text{MW}}=0} = 0$. **e**, Bias voltage V_{in} dependence of the saturation magnetization $4\pi M_{\text{s}}$ obtained from the FMR spectra at $P_{\text{MW}} = 200 \text{ mW}$. The solid line shows $4\pi M_{\text{s}} = 0.814 \text{ T}$. **f**, Bias current J dependence of the magnitude of the electromotive force $V_{\text{ISHE}}(\theta = 0)$ for the $\text{Ni}_{81}\text{Fe}_{19}/p\text{-GaAs}$ system at $P_{\text{MW}} = 200 \text{ mW}$. The error bars represent the 95% confidence level. **g**, Schematic illustrations of the band structure of the $\text{Ni}_{81}\text{Fe}_{19}/p\text{-GaAs}$ system for $V_{\text{in}} < 0$, $V_{\text{in}} = 0$, and $V_{\text{in}} > 0$. ϕ_{S} is the Schottky barrier height. E_{F} is the Fermi level. **h**, Bias voltage V_{in} dependence of the spin-mixing conductance $g_{\text{r}}^{\uparrow\downarrow}$ estimated from the measured voltage $V_{\text{ISHE}}(\theta = 0)$ for the $\text{Ni}_{81}\text{Fe}_{19}/p\text{-GaAs}$ system at $P_{\text{MW}} = 200 \text{ mW}$. We estimated $g_{\text{r}}^{\uparrow\downarrow}$ from the height of a Lorentz function as shown in Fig. 3d; the background voltage due to the ordinary Hall effect is ruled out in this estimation.



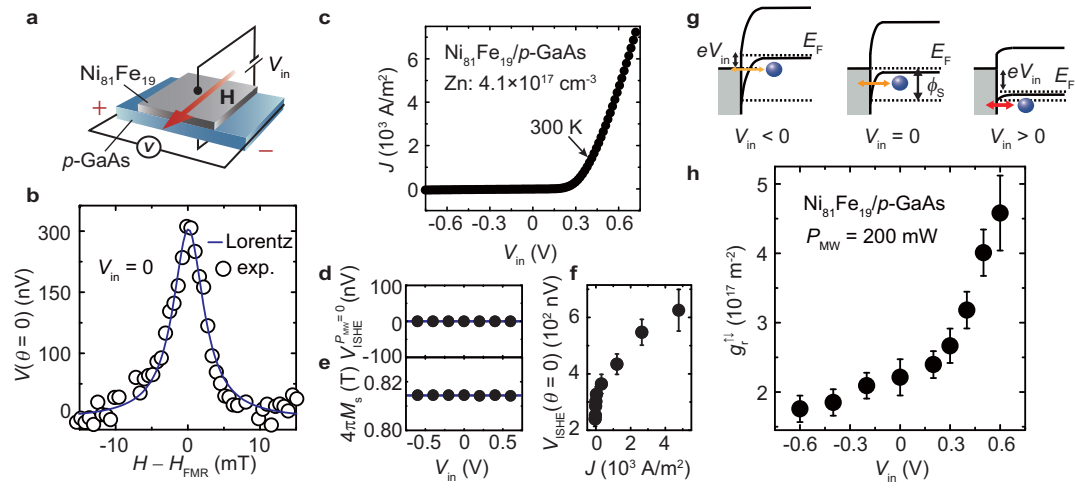
K. Ando *et al.*, Figure 1: Spin injection via carrier transport and dynamical exchange interaction.



K. Ando *et al.*, Figure 2: Dynamical spin injection and inverse spin-Hall effect.



K. Ando *et al.*, Figure 3: Measurements of spin injection.



K. Ando *et al.*, Figure 4: Electric control of dynamical spin injection.